Available online at www.sciencedirect.com
ScienceDirect
International Journal of Thermal Sciences 47 (2008) 514–529
International Journal of Thermal Sciences
www.elsevier.com/locate/ijts

Conjugate response of a thermal boundary layer with reverse flow

Sedat F. Tardu

Laboratoire des Ecoulements Géophysiques et Industriels LEGI, B.P. 53-X, 38041 Grenoble Cédex, France

Received 4 April 2006; received in revised form 25 April 2007; accepted 30 April 2007

Available online 20 June 2007

Abstract

The full numerical solutions of the heat transfer from a flush mounted wall hot-film is carried to investigate its response in reversing flow by taking into account both the axial diffusion and the conduction to the substrate. It is shown that the axial diffusion affects considerably the heat transfer at the reversal points. The numerical results are in good agreement with the experiments conducted in an unsteady water channel. When the conductivity ratio of the substrate to the fluid is high, the response of the film is considerably attenuated, and it is hard to detect the flow reversal phase from the cyclic variations of the global heat flux. The direct flux from the film to the film is relatively less dependent on the conductivity ratio and follows reasonably well the flow reversal.

Keywords: Wall hot film gage; Reversing flow; Axial diffusion; Conduction to the substrate; Response near the flow reversal

1. Introduction

The flow reversal occurs in forced wall flows subject to imposed unsteadiness. The forcing may simply be achieved by a time-varying flow rate or pressure gradient. The typical example is a channel flow forced by imposed velocity oscillations at the centerline. The shear near the wall may change sign during the oscillation cycle, if the imposed amplitude is large enough. The flow reversal may occur with or without unsteady separation, on helicopter blades, in turbomachinery and internal combustion systems, bio-mechanics etc. The flow may be turbulent [1] or laminar. Denoting respectively by $\bar{u}$ and $A_{\tilde{u}}$ the long time average and amplitude of the oscillating velocity field, reverse flow implies that $A_{\tilde{u}} > \bar{u}$. In the near wall region where both $\bar{u}$ and $A_{\tilde{u}}$ vary linearly with the wall normal distance y, the condition $A_{\tilde{u}} > \bar{u}$ is equivalent to $A_{\tilde{\tau}} > \bar{\tau}$, where τ stands for the wall shear stress. Consequently, the presence and characterization of the reverse flow may be done by measurements directly at the wall. The wall hot film gages (WHF) give a rapid diagnostic of flow reversal, but they can not detect the direction of the flow, and their behavior through the response of the thermal boundary layer and its interaction with the edge singularities and the substrate has to be taken into account.

Pedley [2–4] investigated through a series of paper the response of a thermal boundary layer subject to oscillating shear of high amplitude. His investigations were motivated by blood flow in arteries, in particular to interpret the wall hot film gage measurements and the mass transfer phenomena causing the deposition of the lipids and proteins at the wall that is responsible of obstructions and artery hardening. He assumes boundary layer approximation and supposes that during a time interval before and after flow reversal, the process is governed only by diffusion. Thus he neglects the wake, axial diffusion and conduction to the substrate effects. He shows how the asymptotic solution deviates from the quasi-steady solution during the flow reversal when the frequency of the oscillations is high enough. The global flux do not go through zero when the shear vanishes because of inertia. The comparison with the measurements of Seed and Wood [5] reveals however that the minimum reached by the analytical solution at reversal points is significantly smaller than the experimental values essentially because of the axial diffusion that is not taken into account.

Kaiping [6] gives numerical solutions of the problem, once more with the boundary layer approximation and without conduction to the substrate. He argues that axial conduction may be negligible because the reversal period is short compared with the period of the oscillations and the mean Péclet number is high. He shows how the hot wake swept over the film during

E-mail address: sedat.tardu@hmg.inpg.fr.

1290-0729/$ – see front matter © 2007 Published by Elsevier Masson SAS.
doi:10.1016/j.ijthermalsci.2007.04.009

Nomenclature

A_q Amplitude of the quantity q
$a_q = \frac{A_q}{\bar{q}}$ Relative amplitude of the quantity q
a Relative amplitude of the shear parameter
K Number of grid points over the hot-film
k Conductivity, k_F conductivity of the fluid, k_S conductivity of the substrate
$k_S^* = \frac{k_S}{k_F}$ Non-dimensional conductivity of the substrate
l_f Streamwise length of the hot-film
l_f^e Equivalent hot-film length
Nu Nusselt number
$P = \frac{2\pi}{\omega^*}$ Non-dimensional period of the imposed velocity oscillations
$Pr = \frac{\nu}{\alpha}$ Prandtl number
Q_{fF} Direct heat flux from the film (f) to the fluid (F)
Q_{fS} Heat flux from the film (f), to the substrate (S)
Q_{SF}^- Heat flux from the substrate to the fluid upstream of the hot-film
Q_{SF}^+ Heat flux from the substrate to the fluid downstream of the hot-film
$Q = Q_{fF} + Q_{fS}$ Hot-film global heat transfer rate (flux) per unit span
$\bar{q}$ Time mean of the quantity q
$q_w = -(\frac{\partial\theta}{\partial y})_{y=0}$ Local heat flux (Nusselt number)
$q_w^* = -(\frac{\partial\theta}{\partial y})_{y=0}\sigma^{-1/3}$ Non-dimensional local heat flux scaled with the shear parameter
$Re_f = \frac{l_f u_\tau}{\nu}$ Hot film Reynolds number
T Temperature
T_f Film temperature
T_∞ Bulk temperature
$\hat{t}$ Dimensional time
$t = \frac{\hat{t}}{l_f^2}\alpha_F$ Non-dimensional time
$\hat{u}$ Dimensional velocity
$u = \frac{\hat{u}}{u_\tau}$ Non-dimensional velocity
$u_\tau = \sqrt{\frac{\tau}{\rho_F}}$ Shear velocity
$\hat{x}$ Dimensional streamwise distance
x Non-dimensional streamwise coordinate, $x = \frac{\hat{x}}{l_f}$
$\hat{y}$ Dimensional wall normal distance
y Non-dimensional wall normal coordinate, $y = \frac{\hat{y}}{l_f}$

Greek symbols

α Diffusivity, α_F diffusivity of the fluid, α_S diffusivity of the substrate
$\alpha_S^* = \frac{\alpha_S}{\alpha_F}$ Non-dimensional diffusivity of the substrate
δ_T Thermal boundary layer thickness
η Wall normal stretched coordinate
ν Cinematic viscosity
ρ Density, ρ_F density of the fluid, ρ_S density of the substrate
$\sigma = Pr(\frac{l_f u_\tau}{\nu})^2$ Shear parameter
$\bar{\sigma}$ Time-mean shear parameter
$\theta = \frac{T-T_\infty}{T_f-T_\infty}$ Non-dimensional temperature
τ Wall shear stress
$\hat{\omega}$ Dimensional angular frequency of the imposed oscillations
$\omega^* = \hat{\omega}\frac{l_f^2}{\alpha_F}$ Non-dimensional angular frequency
$\omega^+ = \hat{\omega}\frac{\nu}{u_\tau^2}$ Imposed frequency in wall units.
ξ Streamwise stretched coordinate

Abbreviations

BLA Boundary layer approximation (no axial diffusion)
F Fluid
S Substrate
FS Full solution in the fluid with axial diffusion
QS Quasi-steady case (instantaneous Lévêque solution)
A/G Air (Fluid)/Glass (Substrate) configuration
AW Adiabatic wall
W/G Water/Glass configuration
A/M/G Air/Mylar/Glass configuration

Sub-indices

F Fluid
S Substrate
f Hot-film

flow reversal decreases the instantaneous Nusselt numbers at the reversal points.

The validity of the boundary layer approximation is largely open to discussion when the mean Péclet number is small, i.e. either when the streamwise (longitudinal) length of the film and/or the shear are below some critical values. The response of the hot film gage may be severely affected by the axial diffusion at the points where the shear vanishes instantaneously and during the reversal phase. The 2D direct numerical simulations taking into account both the axial diffusion and the conduction to the substrate are reported here. They are compared with the boundary layer and quasi-steady solutions to point out how these parameters modify the response of the wall film. We furthermore confront the numerical results with the experiments conducted in an unsteady water channel and show that they are in reasonable agreement.

2. Numerical model

The dimensional quantities are denoted by $\hat{q}$. The variables in the temperature equations are non-dimensionalised with the streamwise length l_f, by $\frac{l_f^2}{\alpha_F}$ for the time where α_F is the diffusivity of the fluid, and by the shear velocity $u_\tau = \sqrt{\frac{\tau}{\rho_F}}$, with τ being the wall shear stress, and ρ_F the fluid density. The subscripts, F, S and f refer respectively to the fluid, substrate and the film. The non-dimensional temperature is given by $\theta = \frac{T-T_\infty}{T_f-T_\infty}$. The shear parameter is given by $\sigma = Pr(\frac{l_f u_\tau}{\nu})^2 =$

$PrRe_f^2$ where ν is the viscosity, Pr is the Prandtl number and Re_f is the Reynolds number based on the shear velocity and the film length. The non-dimensional frequency is expressed as $\omega^* = \omega\frac{l_f^2}{\alpha_F}$. The velocity distribution in the forced convection heat transfer equation is $u(y,t) = \sigma y(1 + a\sin\omega^* t)$ where $a > 1$, that is reverse flow occurs during the oscillation cycle. The relative amplitude is fixed to $a = 2$.

The non-dimensional equations in the fluid F, in the solid S, and at the fluid–solid (substrate) F–S interface are respectively:

$$F: \quad \frac{\partial\theta}{\partial t} + u\frac{\partial\theta}{\partial x} = \frac{\partial^2\theta}{\partial x^2} + \frac{\partial^2\theta}{\partial y^2} \tag{1a}$$

$$S: \quad \frac{\alpha_F}{\alpha_S}\frac{\partial\theta}{\partial t} = \frac{\partial^2\theta}{\partial x^2} + \frac{\partial^2\theta}{\partial y^2} \tag{1b}$$

$$F\text{–}S: \quad \frac{k_F}{k_S}\frac{\partial\theta_F}{\partial y} = \frac{\partial\theta_S}{\partial y} \tag{1c}$$

The boundary conditions are, $\partial\theta/\partial x \to 0$, and $\partial\theta/\partial y \to 0$, as $x, y \to \infty$, in the substrate; $\partial\theta/\partial x \to 0$ for $x \to \pm\infty$, and $\theta \to 0$ when $y \to \infty$ in the fluid. The sizes of the computational domain are $70l_f$ in the x direction, $6l_f$ in the fluid and $20l_f$ in the substrate, in the y direction.

The upstream weighted differencing formulation for the convective and diffusive terms introduced by Raithby and Torrance [7], together with the stretched coordinates methodology given by Kalnay de Rivas [8] have been combined in an Alternating Direction Implicit (ADI) time discretization scheme. The complete 2D forced convection and conduction equations are coupled at the interfaces and resolved for different fluid/substrate configurations.

Fig. 1 shows the computational domain and the related boundary conditions for a fluid/double-layers substrate configuration. The downstream and upstream distances from the trailing edges and leading edges of the must be large enough so that any particle, which is swept back over the film, during reverse flow, never leaves the computational domain. In order to be safe we took $D_u, D_d \geqslant \int_0^{t_1} u_{\max}(t,y)\,\mathrm{d}t = \int_0^{t_1} H_F\bar{\sigma}(1 + a\cos\omega^* t)\,\mathrm{d}t$ where $u_{\max}$ is the maximum velocity reached in the computational domain in the fluid with thickness H_F and t_1 is the time of the first reversal. Thus, a particle that enters the computational domain at $t = 0$ never leaves it during the oscillation cycles. More details on the computational strategy can be found in Tardu and Pham [9].

Three models will be considered here labeled respectively models A, B and C (Fig. 2). There is no conduction to the substrate in the model A, but the axial diffusion term is maintained in the convective transfer process. This model will be used in Section 4.1 to show the importance of $\frac{\partial^2\theta}{\partial x^2}$ under the reverse flow. That has not been investigated in the literature, and the axial diffusion lay dominate the response of the heat transfer process in particular near the reversal points. Fig. 2 shows the size of the computational domains together with the boundary conditions used. It is seen that the streamwise size of the computational domain extend from $D_u = 50$ to $D_d = 20$ respectively upstream and downstream the film to insure both the condition discussed above and also the imposed condition

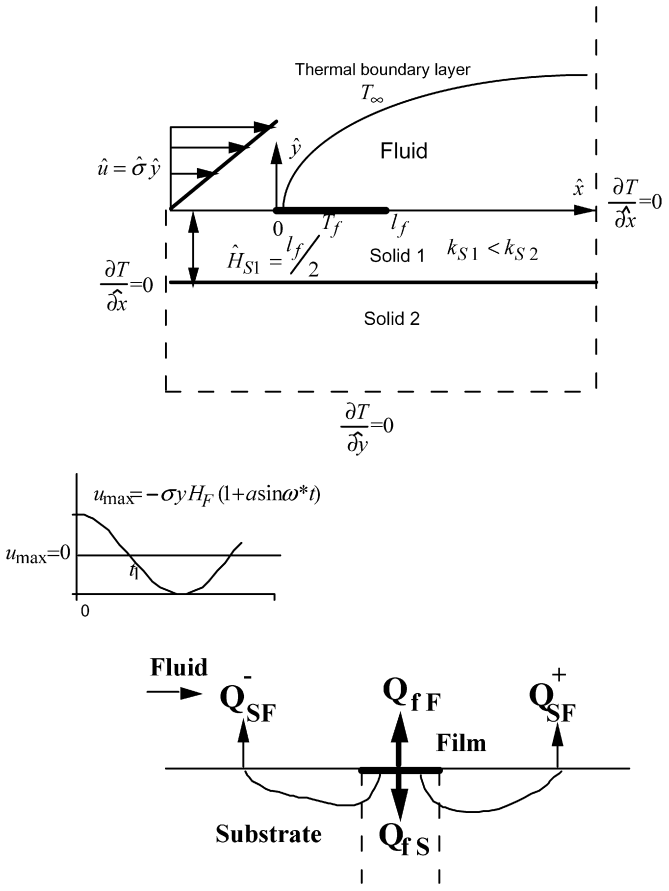

Fig. 1. Computational domain for a mono-layer substrate case and imposed velocity distribution at the highest position in the fluid. Heat transfer rates over the hot film gage are shown on the bottom namely upstream and downstream heat transfer rates from the substrate (S) to the fluid (F) Q_{SF}^- and Q_{SF}^+, direct heat transfer from the film (f) to the fluid Q_{fF}, and heat transfer from the film to the substrate Q_{fS}.

$\frac{\partial\theta}{\partial x} = 0$. It was systematically verified that the streamwise temperature variations are small near the right and left sides boundaries, and the size of domain was increased if this condition is not satisfied. The models B and C are related to the complete conjugated problem with conduction to the substrate and axial diffusion and will be analyzed in Section 4.2. The model B concerns the monolayer substrate. Its thickness was varied from 5 to 30 to insure the $\frac{\partial\theta}{\partial y} = 0$ condition at the bottom. It was found that $H_S = 10$ is sufficient for $\frac{k_S}{k_F} < 30$. The computational domain extends up to $H_F = 6$ in the fluid in this high conductivity ratio regime to satisfy $H_F > \delta_T$. Computations were also carried out for a two-layer substrate configuration (model C, Fig. 2), in which a thin isolating Mylar film of thickness $0.5l_f$ is sandwiched between the hot wall film and the substrate. Such a configuration exists commercially (DANTEC glue-on probe 55R47).

The analysis of heat transfer phenomena near the wall and trailing and leading edges singularities require a dense grid distribution. Stretching coordinates are used to avoid the numerical problems caused by a non-uniform grid distribution. The stretching function in the streamwise x coordinate is $x(\xi) = \sin^2(\frac{\pi}{2}\xi)$ for $0 \leqslant x, \xi \leqslant 1$. The stretching is symmetrical with

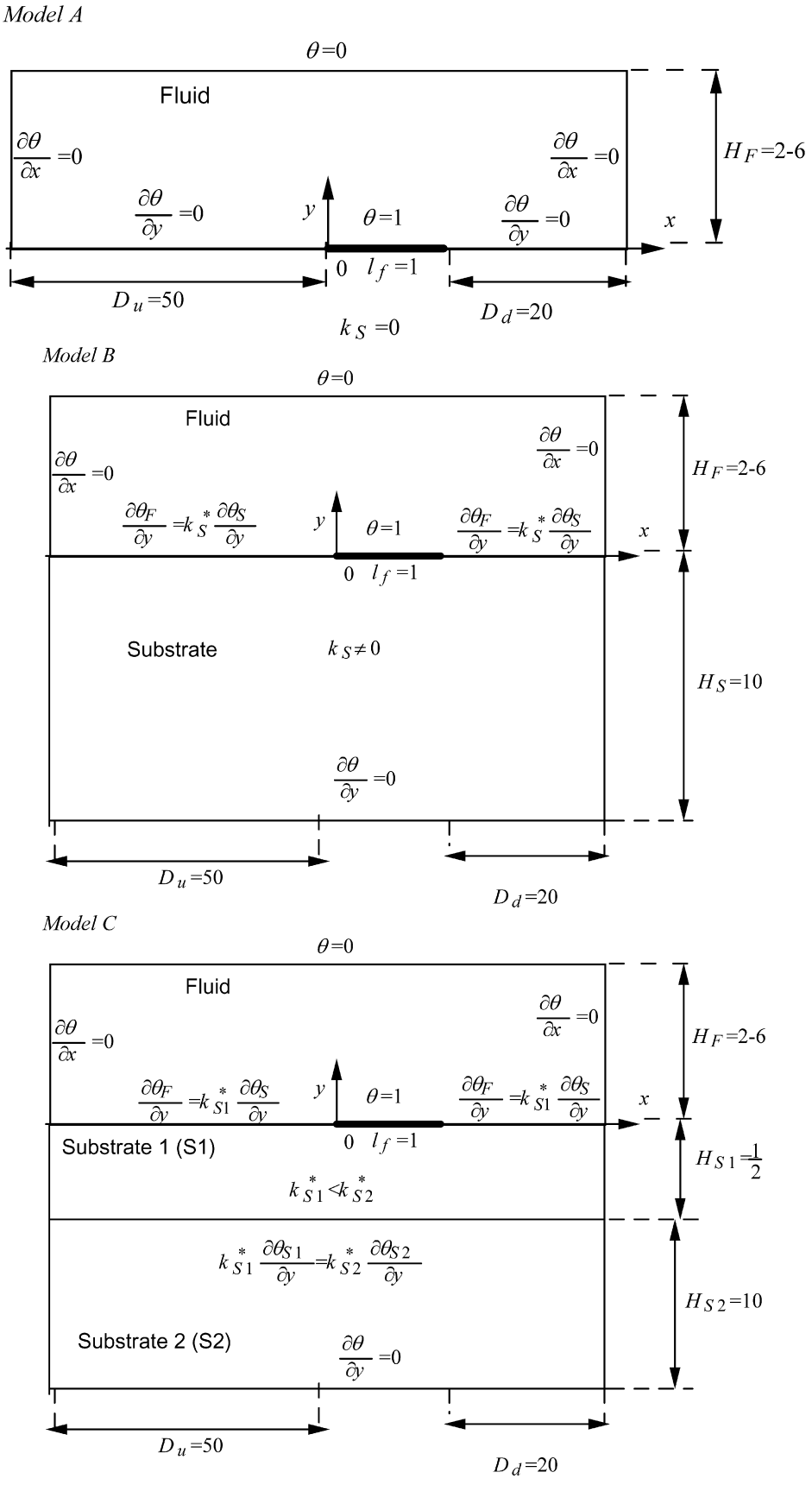

Fig. 2. Models used in this investigation, boundary conditions and size of the associated computational domains.

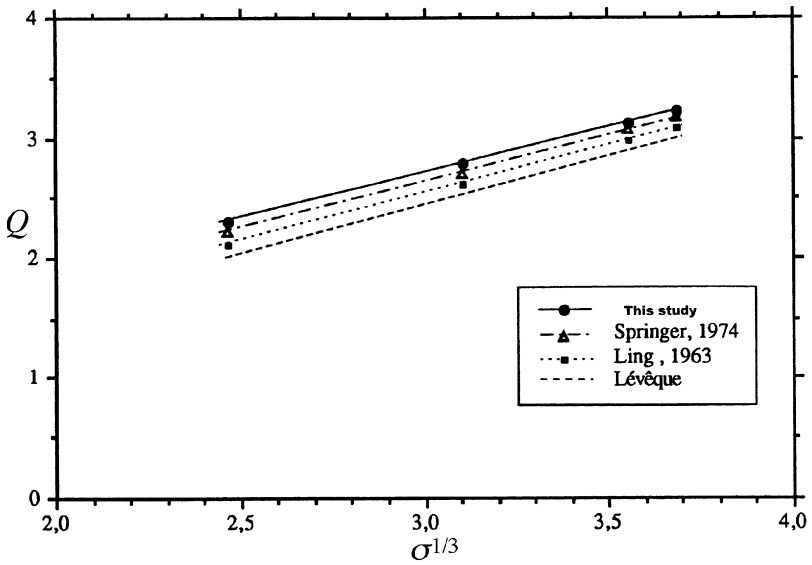

Fig. 3. Global heat flux with the longitudinal diffusion term and comparison with past studies in a steady flow.

respect to the center of the hot film. The smallest grid size near the singularities is $\Delta x = \sin^2[\pi/(4K)]$ where K is the number of grid points on the film. One has $\Delta x \ll 1/K^2$ for a moderate K. The same kind of stretching is used upstream and downstream of the film and it is matched with the coordinate system on the film. The number of grid points used here is typically $K = 22$ resulting in minimum grid spacing at the leading and trailing edge singularities as small as $\Delta x = 10^{-3}$.

The stretching used in the fluid and the substrate following the wall normal direction is stronger and is of the form $y = \eta^2$. Thus for the model shown in Fig. 1 the coordinate transformations are:

$$F: \quad 0 \leqslant y \leqslant H_F;\ 0 \leqslant \eta \leqslant c_F H_F$$

$$y(\eta) = \eta^2/\left(c_F^2 H_F\right)$$

$$S1 \text{ (Solid 1)}: \quad -H_{S1} \leqslant y \leqslant 0; -c_{S1} H_{S1} \leqslant \eta \leqslant 0$$

$$y(\eta) = -\eta^2/\left(c_{S1}^2 H_{S1}\right)$$

$$S2 \text{ (Solid 2)}: \quad -(H_{S1} + H_{S2}) \leqslant y \leqslant -H_{S1}$$

$$-(c_{S1} H_{S1} + -c_{S2} H_{S2}) \leqslant \eta \leqslant -c_{S1} H_{S1}$$

$$y(\eta) = -\left(\eta + c_{S1}^2 H_{S1}\right)^2/\left(c_{S2}^2 H_{S2}\right) - H_{S1}$$

with the coefficients c_F, c_{S1} and c_{S2} can be changed to adapt the stretching to different zones. The maximum resolution is at the interfaces where the derivative $\mathrm{d}y/\mathrm{d}\eta = 0$. The first mesh in the fluid and the solid is typically at $\Delta y = 7 \times 10^{-3}$ in this investigation. The upstream weighting difference and ADI problems are formulated in the (ξ, η) domain and the resolution of the resulting system is done by the classical Thomas algorithm.

Several tests have been conducted both in steady and unsteady flow configurations and comparisons have been made with existing analytical and numerical approaches. One of the comparisons we made concerns the heat transfer process over the small strip under the influence of the axial diffusion without the effect of the conduction to the substrate More clearly Eq. (1a) is solved in steady flow by keeping $Q_{fS} = 0$ to test the accuracy of the mesh resolution in particular at the trailing and leading edge singularities. Fig. 3 shows $Q = Q_{fF}$ versus the shear parameter $\sigma^{1/3}$ and compares the results obtained here with the theoretical work of Springer [10] and the computations of Ling [11]. There is an excellent agreement with the asymptotic analysis of Springer and Pedley [10] and Springer [12], and the differences between the computations and these theoretical approaches are less than 1%. The code was also tested by investigating the exact 1D time dependent three-layer case of Bellhouse and Schultz ([13], F–S–F, with solid thickness l_f and with the same flow on both sides of the solid slab). Excellent agreement is found for this case too [9, Fig. 12, p. 817]. 1D models and simplifications such as those made by Freymuth [14] and recently used by Teo et al. [15] are however limited because the effect of longitudinal diffusion in the fluid and in the solid (which is, of course, inherently neglected in the 1D solutions) rapidly attenuates the frequency response and the attenuation starts at a frequency which is one order of magnitude smaller than in the 1D solution. These effects are particularly important when the Péclet number is small. The reader is referred to Tardu and Pham [9] for detailed discussions of these effects. The aim of the present study is to precisely investigate these effects under reverse flow conditions.

Some comments have to be made now to precise the physical model used in the fluid and given by Eq. (1a). The first hypothesis used here is that the only parameter of the fluid flow affecting the film heat transfer is the wall shear, i.e. that the velocity profile is effectively linear through $\hat{u} = \hat{\sigma}\,\hat{y}$ in the region where the fluid temperature varies between its value at the film to the value of the incoming fluid. This relationship is valid in the viscous sublayer both for the mean and fluctuating longitudinal velocity in a boundary layer type of flow. Therefore the hypothesis given above is equivalent to suppose that the viscous sublayer thickness is larger that the maximum thermal boundary layer thickness at the trailing edge of the hot film. This implies that the maximum thermal boundary layer thickness $\delta_{T\max}$ over the hot film should be $\delta_{T\max} \leqslant 5\frac{\nu}{u_\tau}$. Taking the classical

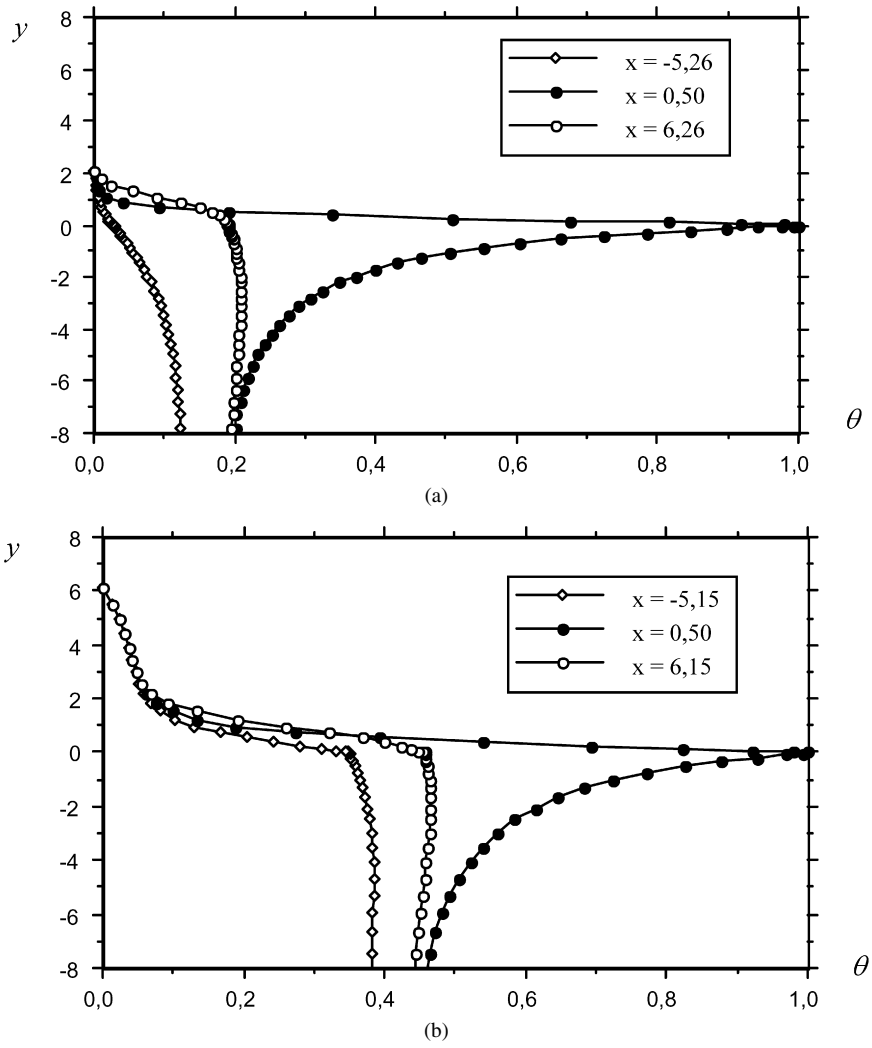

Fig. 4. Temperature distribution in the fluid and substrate in a steady flow with $\sigma = 30$ at different streamwise locations, (a) $\frac{k_S}{k_F} = 1.3$, $\frac{\alpha_S}{\alpha_F} = 2.4$, (b) $\frac{k_S}{k_F} = 25$, $\frac{\alpha_S}{\alpha_F} = 0.017$.

Lévêque solution corresponding to the solution of Eq. (1) without axial diffusion and thermal inertia terms gives the condition $\delta_{T\max}\frac{u_\tau}{\nu} = (\frac{9}{2}Re_f)^{1/3} \leqslant 5$ where $Re_f = \frac{l_f u_\tau}{\nu}$ is the hot film Reynolds number (see the nomenclature). The typical value of Re_f of the commercial hot films is about 6 (at low Reynolds numbers of about 10^3 in water) although the micro technology allows the realization of micro wall sensors of Re_f an order of magnitude smaller than one nowadays (see for example Meunier et al. [16]). One has therefore typically $\delta_{T\max}\frac{u_\tau}{\nu} = 3$ for $Re_f = 6$ which is twice smaller than the viscous sublayer thickness and $\delta_{T\max}\frac{u_\tau}{\nu} = 1.6$ for $Re_f = 1$.

The situation is more complex under the influence of the axial diffusion and conduction to the substrate. Both effects may increase significantly the thermal boundary layer thickness over and downstream the hot film, especially for large $\frac{k_S}{k_F}$ conductivity ratios. This particular point has been recently discussed in some detail by Tardu and Pham [9]. Figs. 4(a) and (b) show the temperature profiles over ($x = 0.5$), upstream ($x = -5$) and downstream ($x = 6$) the film for respectively $\frac{k_S}{k_F} = 1.3$, $\frac{\alpha_S}{\alpha_F} = 2.4$, and $\frac{k_S}{k_F} = 25$, $\frac{\alpha_S}{\alpha_F} = 0.017$ at $\sigma = 30$ in a steady flow configuration. These cases correspond to respectively the water (fluid)/glass (substrate) and air/glass configurations. For small $\frac{k_S}{k_F}$ ratios the thermal boundary layer thickness ($\theta \geqslant 0.05$) is about $\delta_T \approx l_f$, implying the condition $Re_f \approx 5$ to be sure that δ_T is within the viscous sublayer (Fig. 4(a)). This is approximately the case in the experiments conducted here and described in the next session. Moreover, the thermal boundary layer thickness increases up to $\delta_T \approx 2.5 l_f$ when $\frac{k_S}{k_F} = 25$ (Fig. 4(b)) and one should respect $Re_f \approx 2.5$ under these circumstances. Thus, the common hypothesis that the flow is mainly governed by the wall shear and found in previous related studies outlined in the Introduction, can be acceptable as long as the Reynolds number of the small strip is $Re_f \approx 5$–2 depending on the conductivity ratio. The effect of the streamwise dependence has to be taken into account for larger Re_f for which 3D direct numerical simulations are necessary.

It is also assumed in the convective heat transfer process that the longitudinal convection $u\frac{\partial\theta}{\partial x}$ dominates the lateral convection $v\frac{\partial\theta}{\partial y}$, i.e. that the normal component is effectively zero within the thermal boundary layer. In a classical boundary layer

flow wherein the origins of velocity and temperature boundary layers coincide, $u\frac{\partial\theta}{\partial x}$ and $v\frac{\partial\theta}{\partial y}$ are of the same order of magnitude and the second can never be neglected. In the case of a small strip located at $x = l_b$ of the velocity boundary layer edge of the order of magnitude of $v_{\delta T}$ within the thermal boundary layer is $\frac{\delta_T}{l_b}u_{\delta T}$, with $u\frac{\partial\theta}{\partial x} \cong u_{\delta T}\frac{\theta}{l_b}$, $v\frac{\partial\theta}{\partial y} \cong v_{\delta T}\frac{\theta}{\delta_T}$ and consequently $\frac{v\frac{\partial\theta}{\partial y}}{u\frac{\partial\theta}{\partial x}} \cong \frac{l_f}{l_b}$. Thus, the lateral convection can be neglected when the wall film is located sufficiently far away from the leading edge of the velocity boundary layer, i.e. when $\frac{l_f}{l_b} \ll 1$. On the other hand, in a fully developed internal flow, the mean wall normal velocity is equal to zero and only the time mean longitudinal convection subsists.

The originality of the present work compared to previous investigations lies on the effect of both the axial diffusion and the conduction to the substrate on the response of a thermal boundary layer in the presence of reverse flow. To be clear, the boundary layer approximation as applied to Eq. (1a) without the axial diffusion:

$$\frac{\partial\theta}{\partial t} + u\frac{\partial\theta}{\partial x} = \frac{\partial^2\theta}{\partial y^2} \tag{2}$$

and without the conduction to the substrate will be called the boundary layer approximation (BLA). Furthermore, the special case of BLA wherein the thermal inertia $\frac{\partial\theta}{\partial t}$ is neglected with:

$$u(y,t)\frac{\partial\theta}{\partial x} = \frac{\partial^2\theta}{\partial y^2} \tag{3}$$

will be called the quasi-steady case (QSC). That clearly corresponds to the BLA in the low imposed frequency regime. In QSC, the thermal boundary layer is supposed to be in equilibrium at each time during the oscillation cycle.

3. Experiments

The experiments were performed in the unsteady water channel described in detail in Tardu et al. [1]. The sinusoidal velocity oscillations are generated by means of a specific pulsating device that allows the independent control of the mean centerline velocity, the amplitude and frequency of the imposed unsteadiness. The centerline velocity is $U_c = 17.5$ cm/s corresponding to a Reynolds number based on the half height of the channel of $Re_h = \frac{U_c h}{\nu} = 8800$. The imposed frequency in wall units $f^+ = f\frac{\nu}{u_\tau^2}$ varied by a factor 24 from $f^+ = 2.2\times10^{-4}$ to $f^+ = 60\times10^{-4}$. Hereafter + designates variables normalized by the cinematic viscosity ν and shear velocity.

The wall shear stress measurements were performed by means of a flush-mounted TSI-1268 W hot film at the wall. The sensitive part of the hot film is $6\frac{\nu}{u_\tau}$. The sensor was operated at constant temperature with 5 to 8% overheat by AHARONI AN-1003 anemometer units. The calibration was done in situ as described by Tardu et al. [1]. The quality of the wall shear stress measurements was checked by comparing the statistics of the fluctuating wall shear stress $\tau'(t)$ in steady canonical channel flow with existing data. The results obtained at $Re_h = 8800$ are summarized in Table 1. It is seen that $\sqrt{\tau'\tau'}$ is 0.38 times the wall shear stress τ in agreement with 0.36 found from the direct numerical simulation data of Kim et al. [17]. The high order statistics, i.e. the skewness $S_{\tau'} = \frac{\overline{\tau'^3}}{(\overline{\tau'^2})^{3/2}}$ and the flatness $F_{\tau'} = \frac{\overline{\tau'^4}}{(\overline{\tau'^2})^2}$ of $\tau'(t)$ were also measured. It was found that, in steady flow, $S_{\tau'} = 1.15$ and $F_{\tau'} = 4.20$. These values agree also well with Kim et al. [17]. The time mean statistics in unsteady flow are shown in the last column of Table 1. No trend was observed as the frequency varied, thus confirming the insensitivity of the mean flow to imposed unsteadiness.

Table 1
Time mean statistics of the turbulent fluctuations of the wall shear stress in steady and unsteady flow

	Steady flow This study	Steady flow Kim et al. [17]	Unsteady flow This study
$\frac{\sqrt{\tau'\tau'}}{\bar{\tau}}$	0.38	0.36	0.36–0.41
$S_{\tau'} = \frac{\overline{\tau'^3}}{(\overline{\tau'^2})^{3/2}}$	1.15	1.00	0.95–1.25
$F_{\tau'} = \frac{\overline{\tau'^4}}{(\overline{\tau'^2})^2}$	4.20	4.00	3.80–4.20

Comparison with existing data. Fully developed turbulent channel flow with $Re = 8800$.

The analog to digital conversion was achieved with an Analog-Device RTI-800 board (accuracy 11 bit+ sign; 8 channel) installed in a PC computer. The sampling frequency was $1.5\frac{u_\tau^2}{\nu}$. The signals were filtered with accurate cut-off frequencies. The minimum record length was $T_r = 9200\frac{h}{U_c} = 191\times10^3\frac{\nu}{u_\tau^2}$ for each signal which means about forty-five minutes for each experiment. This gives a total number of 286,000 data points per probe.

The classical triple decomposition is used. A quantity q is decomposed into a mean $\bar{q}$ an oscillating $\tilde{q}$ and fluctuating q' components. The angle brackets designate the phase averages i.e. $\langle q\rangle = \bar{q} + \tilde{q}$.

One of the particularity of unsteady forced turbulent channel flows is the coexistence of a time-mean flow which is not affected by the imposed unsteadiness and an oscillating viscous Stokes flow when the frequency of the oscillations is larger than the median frequency of the near wall turbulence. These details are not in the scope of this paper and the reader may consult Tardu et al. [1] and Tardu and Binder [18] the references given in these papers. The point that is concerned by the present investigation is that reverse flow occurs in these flows when the imposed amplitude and the frequency are large enough. Two series of wall shear stress measurements both corresponding to amplitude of $a = 2$ and the frequencies $\omega^* = 0.46$ and $\omega^* = 0.93$ will later be compared with the numerical results in this paper.

4. Results and discussion

The effect of the axial diffusion and the conduction to the substrate will be separately analyzed in this session. A special session is devoted to the effect of axial diffusion alone since it has been systematically omitted in the past-published stud-

ies. The model investigated in Section 4.1 is the model A of Fig. 2 in which there is no conduction to the substrate. It will be shown in this session that the term $\frac{\partial^2\theta}{\partial x^2}$ plays an important role during the phase reversal and that it cannot be neglected, especially when the mean Péclet number is small as is the case here ($\sigma = 10$). Section 4.2 is devoted to the entire conjugate problem with conduction to the substrate and $\frac{\partial^2\theta}{\partial x^2}$ through the models B and C of Fig. 2.

4.1. Effect of the longitudinal diffusion

4.1.1. Temporal evolution of the local temperature gradient

This section deals with the analysis of the local non-dimensional temperature gradient during the oscillation cycle $\sigma(t^*) = \bar{\sigma}(1 + a\cos\omega^* t^*)$ with $t^* = t/T$ and T is the period of the oscillations. Computational results obtained with a mean Péclet number $\bar{\sigma} = 10$ and a relative amplitude of $a = 2$ are presented. The imposed frequency is fixed to $\omega^* = \bar{\sigma}\omega^+ = 10$ where $\omega^+ = \omega\frac{\nu}{u_\tau^2}$. The parameter ω^+ is introduced in order to be consistent with the inner scaling based on ν and u_τ in a turbulent boundary layer. It is interesting to note that ω^+ investigated in this sub-section is nearly half of the Kolmogoroff frequency in the buffer layer (Ueda and Hinze, [3]). Under the experimental conditions presented in Section 3, $\omega^* = 10$ corresponds to $\omega = 10$ Hz in physical units.

The local temperature gradient is presented in the form $q_w^*(t^*) = (\frac{\partial\theta}{\partial y})_{y=0}(t^*, x)\sigma(t^*)^{-1/3}$ versus the non-dimensional distance $x = \frac{x}{l_f}$ from the leading edge of the wall film in Figs. 5 and 6. This presentation is preferred, because it makes the quasi-steady Lévêque solution independent of the shear parameter $\sigma(t^*)$. The Lévêque solution is plotted in each figure, as a reference and in order to put the accent on strong departures from quasi-steadiness during the oscillation cycle. The results inferring from boundary layer approximation which neglects the effects of $\frac{\partial^2\theta}{\partial x^2}$ are also given and compared with the solution of the complete transfer equation. A sketch which shows the corresponding time t^* in the oscillation cycle is added at the top of each figure, in order to facilitate the reading. The previous results inferred from a fully explicit numerical scheme (Tardu et al., [19]) are in excellent agreement with the solutions of the full equation obtained here and they are not shown.

Figs. 5(a)–(c) focus on the decelerating part of the oscillating shear. At $t^* = 0.22$, before the first reversal, the effect of the thermal inertia is already felt over the hot film and that explains why the profile corresponding to the boundary layer approximation is slightly above the quasi-steady solution (Fig. 5(a)). The full equation, which combines the effects of the thermal inertia and the singularities at the leading and trailing edges, shows that the quasi-steady solution underestimates the overall heat flux by 11%. The axial diffusion becomes progressively important at $x < 0.1$ near the leading edge and $x > 0.9$ near the trailing edge.

The true strong unsteady effects are particularly significant after the first reversal. Fig. 5(b) shows the local temperature gradient at $t^* = 0.34$ ($\sigma(t^*) = -0.7$). Note that the leading and trailing edges are now respectively at $x = 1$ and $x = 0$, since the direction of the flow is from right to left. The computed boundary layer approximation (BLA) curve shows a behavior that is completely different from the corresponding quasi-steady case (QS). Owing to the thermal inertia, the local temperature gradient profile has still his memory of before reversal. The leading edge had not enough time to move at $x = 1$. Large differences are due to the irregularity of the temperature field. The full solution (FS) corresponding to Eq. (1a) with all the terms is qualitatively similar, but there are large quantitative differences due essentially to the axial diffusion. Note that, the range of x within which the FS coincides with the boundary layer approximation is restricted only to $0.4 < x < 0.70$. while this range is wider sufficiently far away from reversal instants (Fig. 5(a)). The axial diffusion increases therefore the inertia by some feedback mechanism near the reversal points. Close inspection of the results shows the important increasing effect of $\frac{\partial^2\theta}{\partial x^2}$ on the mean Nusselt number taken over the film when $\sigma(t^*) \approx 0$, especially near the trailing edge which is still at $x = 1$ at this particular time in the oscillation cycle.

Fig. 5(c) recapitulates the results obtained at $t^* = 0.5$, i.e. when the shear reaches its minimum. There are essentially two phenomena in the phase of flow reversal: the thermal inertia and the thermal wake effects, i.e. the heated fluid is swept back over the film. The second may dominate the transfer phenomena in the phase $\sigma(t^*) < 0$ if the wake has enough time to affect significantly the temperature field near the film and to overcome the inertia. This explains why the local temperature gradient inferred from the boundary layer approximation is lower than the quasi-steady solution in Fig. 5(c), especially near the leading edge which is now shifted to $x = 1$. In the vicinity of the trailing edge, in return, the BLA differs only slightly from the QSC. That is due to the high local gradient inferred from the boundary layer solution in the previous phases (Fig. 5(b)), so that, in this zone the wake effect may only compensate the thermal inertia. The effect of the singularities at the beginning and the end of the hot film is spectacular at this stage as it is clearly seen in Fig. 5(c). Due to the axial diffusion, the local gradient increases by a factor 5 compared with the BLA at the trailing edge. The presence of $\frac{\partial^2\theta}{\partial x^2}$ overcomes largely the wake effect almost everywhere over the film.

Two cases will shortly be discussed concerning the accelerating part of the oscillation cycle. Fig. 6(a) shows the distribution of q_w^* at $t^* = 0.6$ immediately after the occurrence of the minimum shear. It is seen that the wake effect discussed previously, is now compensated by inertia, and that, consequently the BLA compares well quantitatively with the QS. After the second reversal at $t^* = 0.74$ (Fig. 6(b)) the local gradient of the boundary layer approximation is almost uniform except very near the leading edge at $x = 0$. In both cases the FS is reminiscent of a net increase of the overall Nusselt number.

Presumably, the local temperature gradient results from a negotiation between the thermal inertia, the wake effects and the axial diffusion. The former dominates q_w^* near the reversal points as it could be expected. The wake effect, which is predominant during the reversal phase, is seen to be negligible when the axial diffusion is taken into account.

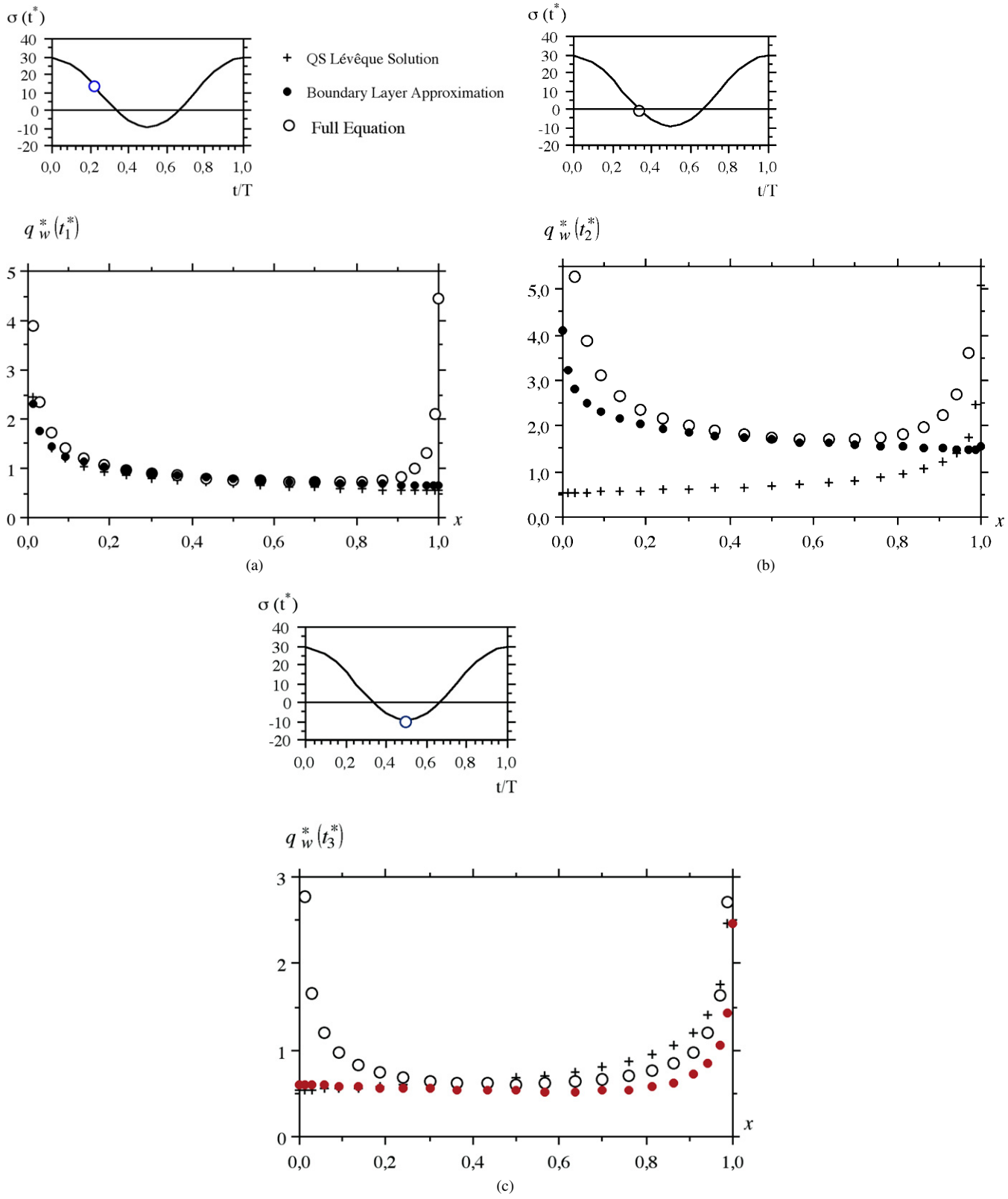

Fig. 5. Local temperature gradient during the deceleration phase. For legend see (a) $\omega^* = 10$, $\sigma = 10$, $a = 2$. $t_1^* = 0.22$, $t_2^* = 0.34$, $t_3^* = 0.5$, $\sigma(t_1^*) = 13.5$, $\sigma(t_2^*) = -0.75$, $\sigma(t_3^*) = -10$.

4.1.2. Temporal evolution of the overall heat transfer

This sub-section is devoted to the analysis of the normalized overall Nusselt number $Q^*(t^*) = Q(t^*)\sigma^{-1/3}$, where $Q(t^*) = \int_0^1 (\frac{\partial\theta}{\partial y})_{y=0}(t^*, x)\,\mathrm{d}x$. According to this representation, the quasi-steady Lévêque solution reads simply $Q^*_{QS}(t^*) = 0.8075(1 + a\cos\omega^* t^*)^{1/3}$. It is worth saying that the total

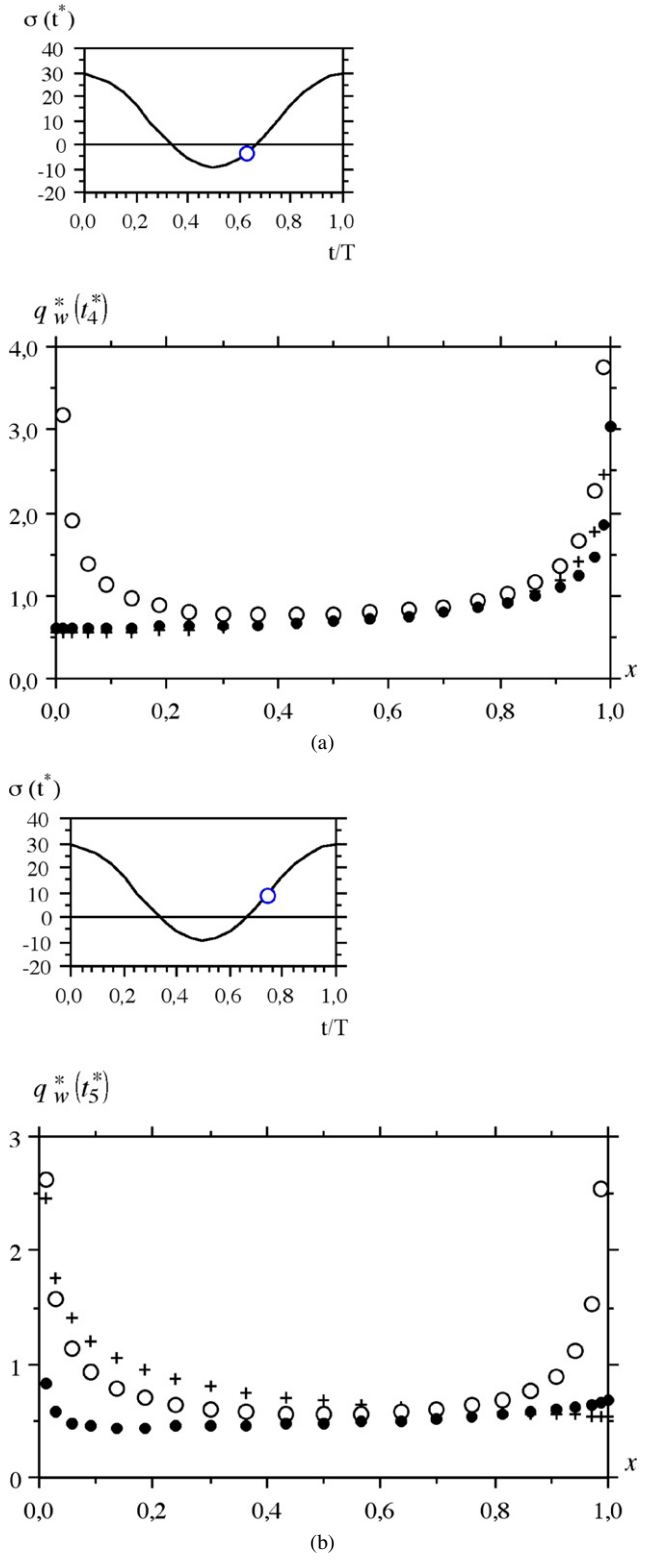

Fig. 6. Local temperature gradient during the acceleration phase. For legend see Fig. 5(a). $\omega^* = 10$, $\sigma = 10$, $a = 2$. $a - t_4^* = 0.6$; $\sigma(t_4^*) = -3.9$, $b - t_5^* = 0.74$; $\sigma(t_4^*) = 8.5$.

non-dimensional heat flux $\langle Q^*(t^*)\rangle$ modulation is particularly important, since it is directly related to the wall shear stress measured by hot-film techniques in unsteady reversing flows, as it will be discussed in the next section.

We first present computed results corresponding to a significantly high-imposed frequency $\omega^* = 10$ in Fig. 7(a). These results are obtained after 10 cycles of oscillation. Even the boundary layer computation does only slightly show the first flow reversal at this frequency, while the second reversal is more pronounced. The full solution shows no apparent sign of flow reversal. The longitudinal diffusion increases the time mean Nusselt number $\overline{Q}^* = \int_0^1 Q^*(t^*)\,\mathrm{d}t^*$ by 30% and the differences between the full equation and the boundary layer approximation are almost 50% near the reversal points. The instantaneous Q^* at the end of the cycle is equal to the value at the beginning, showing that the full periodicity is reached. The phase lag, which is due to the thermal inertia effects, is more important during deceleration than during flow acceleration.

The axial diffusion entirely dominates the response of the thermal boundary layer even when the imposed frequency is two times smaller, i.e. when $\omega^* = 5$. Indeed, it is still hard to deduce from the $Q^*_{\mathrm{FS}}(t^*)$ profile of the full solution shown in Fig. 7(b) that the flow is reversing (here the subscript FS refers to the full equation). In return, the boundary layer approximation is now reminiscent of both the first and second reversals. Furthermore, the comparison with Kaiping [6] who investigated only the boundary layer approximation shows good agreement with our BLA computations, despite the differences in the numerical schemes used in both studies. Owing to the thermal inertia, there is an important phase lag between the boundary layer approximation and the QSC. Finally, Figs. 7(a) and (b) show clearly that the overall Nusselt number inferring from the full equation is far being quasi-steady during the phase wherein the shear stress is negative. The axial diffusion increases somewhat the inertial effects in agreement with the discussion made in the previous section.

The reversal phase appears clearly from the full solution when the imposed frequency is sufficiently small. We determined that the limiting value of the frequency parameter for the fulfillment of this condition is about $\omega^* \leqslant 4.5$. This limit is much higher than the maximum imposed frequency corresponding to the majority of the existing measurements in unsteady turbulent reversing near wall flows [1], although a few measurements up to exist in the literature [18]. This point will be discussed in the next section in some detail. Recall however that the heat conduction to the substrate is not yet taken into account and it can deteriorate the reversal phase detection when $\frac{k_S}{k_F}$ is large as we will show in Section 4.2. It is interesting to investigate by now the response of the thermal boundary layer in the low imposed frequency range. Fig. 7(c) shows the normalized overall Nusselt number during the oscillation cycle at $\omega^* = 0.5$. At this small value of the non-dimensional frequency parameter, it is seen that the full solution shows more clearly the existence of the reversal phase. The difference between the complete solution and the boundary layer approximation is remarkable near the reversal points as before and is as important as 50%. The quasi-steady distribution shown by squares in Fig. 7(c) correspond to those inferred from Ackerberg et al. [20]. These values were computed by using their results at the corresponding instantaneous Péclet number $\sigma(t^*)$. Recall that Ackerberg et al. have taken into account the axial

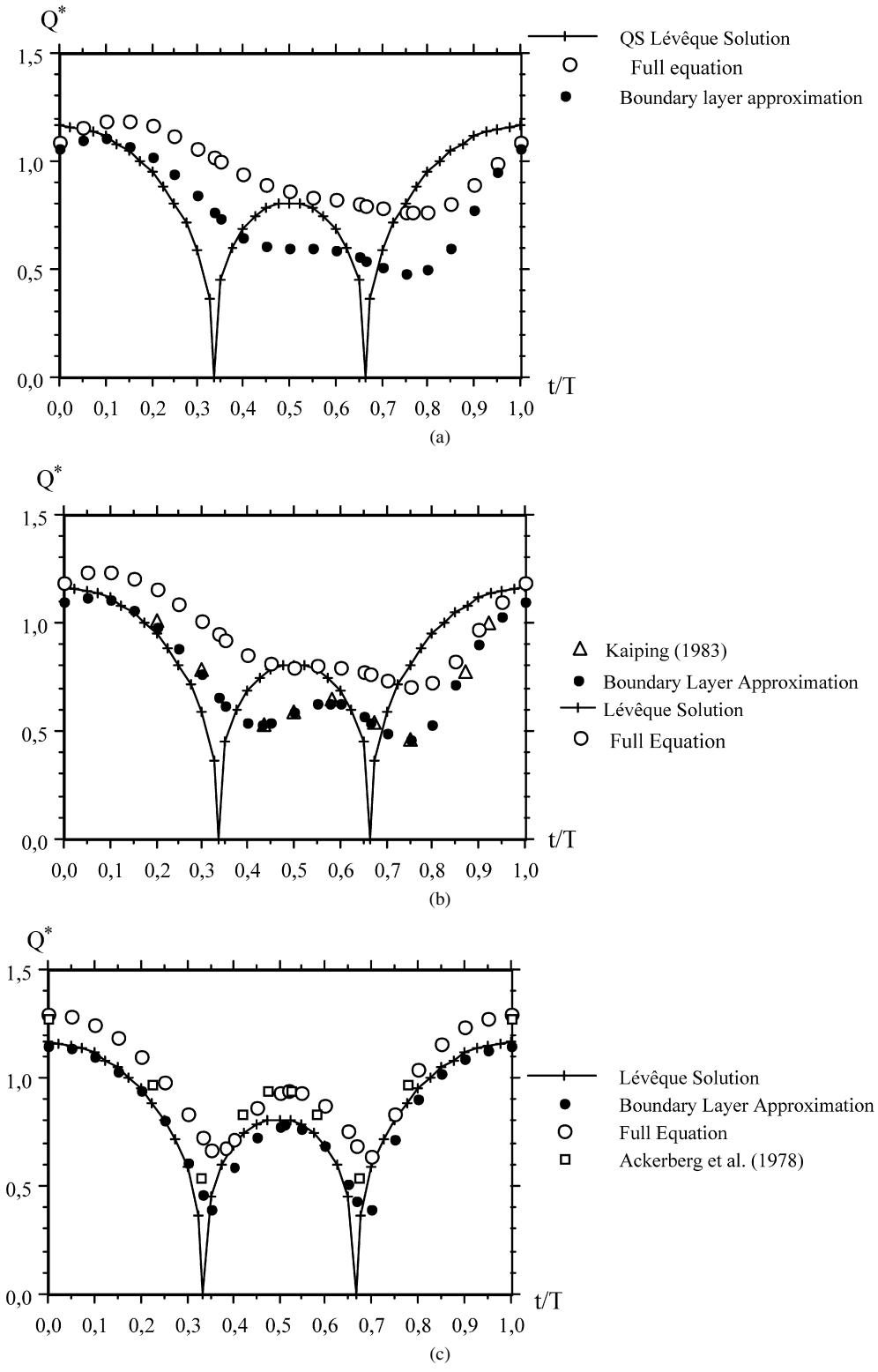

Fig. 7. Cyclic variation of the global heat transfer. $\sigma = 10$, $a = 2$. $a - \omega^* = 10$, $b - \omega^* = 5$, $c - \omega^* = 0.5$.

diffusion in their steady-state analysis. Therefore, their results are presumably the "real" quasi-steady Nusselt number at the given t^*. It is seen that, despite some discrepancies in the decelerating and accelerating phases, the quasi-steadiness is approximately reached, in particular in the middle of the reversal phase. This point is important in the interpretation of the indirect wall shear stress measurements in unsteady flows, and this will be discussed in the next section. Note finally that the thermal inertia is still important in this low frequency regime, since the differences between $Q^*_{\mathrm{FS}}(t^*)$ and the quasi-steady values are somewhat significant near the flow reversals. The thermal boundary layer "forgets" the effect of flow reversal relatively

rapidly at $\omega^* = 0.5$ and reaches progressively its quasi-steady temporal equilibrium as the shear stress increases (or decreases) slowly from zero.

4.2. Effect of the conduction to the substrate

The conduction to the substrate attenuates considerably the response of the hot film during the flow reversal. Fig. 8 shows the cyclic variation of the total flux $Q^*/Q^*(t^* = 0)$ for respectively an adiabatic wall (AW), the Air (Fluid F)/Glass (Substrate S) case, with conductivity and diffusivity ratios $k_S/k_F = 25.3, \alpha_S/\alpha_F = 17 \times 10^{-3}$, the Water/Glass (W/G, $k_S/k_F = 1.27, \alpha_S/\alpha_F = 2.38$) and the two-layer substrate case Air/Mylar/Glass (A/M/G). The total flux varies considerably from one case to other depending on the importance of the conduction to the substrate and Q^* is scaled with by its value at the beginning of the oscillation cycle $Q^*(t^* = 0)$ to show legibly the data. The imposed frequency is $\omega^* = 0.93$ and is quite high with respect to the quasi-steady limit. Recall indeed, that the quasi-steadiness requires $\omega^* \ll 2\pi(\frac{l_f}{l_f^e})^2\frac{\alpha_S}{\alpha_F}$, through the effective length l_f^e of the hot film. For $\bar{\sigma} = 10, l_f^e/l_f = 18$ and 9 for the homogeneous, and two-layer substrates. The quasi-steadiness can then be reached when $\omega^* \ll 3 \times 10^{-4}$ and $\omega^* \ll 4 \times 10^{-4}$.

It is seen from Fig. 8 that the scaled total flux variations are close to the adiabatic case when the conductivity ratio is small such as in the W/G case. The modulation of the indirect transfer to the substrate Q_{fS} is close to the quasi-steady cyclic variation, with $Q_{fS} \propto \sigma^{0.1}$ except near the reversal points where it is small but does not vanish. The direct transfer Q_{fF} follows relatively well the adiabatic solution.

One has to be careful to discern the reversal in the presence of important conduction to the substrate. During the reversal phase, the maximum $Q^*/Q^*(t^* = 0)$ differs from the minimum by 24% for an adiabatic wall, sensibly the same amount for W/G, 3% for the two-layer substrate with thin isolating mylar film and only 1% for the mono-layer substrate. The response of the hot-film seems frozen during the oscillation cycle, and a "zoom" of factor 3 is necessary to detect the reversal phase (Fig. 9, please be aware of the scale differences at the left and right of this figure). Note on the other hand that although the phase reversal is detectable in the A/G case from the cyclic variations of Q^* the amplitude raise after the first reversal point is roughly 50% smaller than the adiabatic case. Thus, the reversal phase becomes to be distorted under the effect of high conductivity to the substrate already at $\omega^* = 0.93$, even though still perfectly discernible in $\langle Q^* \rangle$ by a sufficiently close look.

The effect of the thermal wake during the flow reversal is accentuated by the presence of indirect upstream (Q_{SF}^-) and downstream (Q_{SF}^+) heat transfers (Fig. 1). The attenuation of the direct flux is consequently more important during the flow reversal with conduction to the substrate. Yet, the reversal phase is more perceptible from the cyclic variation of the direct transfer from the film to the fluid Q_{fF} (Fig. 10). The heat transfer from the film to the substrate is indeed relatively frozen during the oscillation cycle due to the large relaxation time of the conduction process. Fig. 11 shows the cyclic variation of $\frac{\langle Q_{fS} \rangle}{\overline{Q}_{fS}}$ for the configuration A/G at $\omega^* = 0.93$ and $\omega^* = 0.46$. The mean flux to the substrate is large, respectively $\overline{Q}_{fS}^* = 5.5$, and $\overline{Q}_{fS}^* = 5.4$ for $\omega^* = 0.93$ and $\omega^* = 0.46$. However, the relative amplitude of $\langle Q_{fS} \rangle$ is only 0.3%. Consequently the modulation of $\tilde{Q}_{fS} \approx 0$ and the transfer to the substrate can roughly be considered constant during the oscillation cycle, for these cases. Consequently, $\langle Q \rangle = \langle Q_{fF} \rangle + \langle Q_{fS} \rangle \approx \overline{Q}_{fF} + \overline{Q}_{fS} + \tilde{Q}_{fS}$, and the cyclic modulation of the total heat transfer is approximately $\tilde{Q} = \tilde{Q}_{fF}$ under the present conditions. That explains why there is a relatively good collapse in the zoom of Fig. 6, even though conduction to the substrate decreases by 50% the rise in amplitude after the first reversal as pointed at before.

Fig. 12 presents the non-dimensional shear stress that would be determined from the measurements of Q_{fF}. The procedures of conversion from the flux to the shear and inversion are as follows. Sufficiently far away from the reversal point, for instance at the maximum value of σ, the total heat flux is close to its quasi-steady values. Thus, the numerical results are calibrated

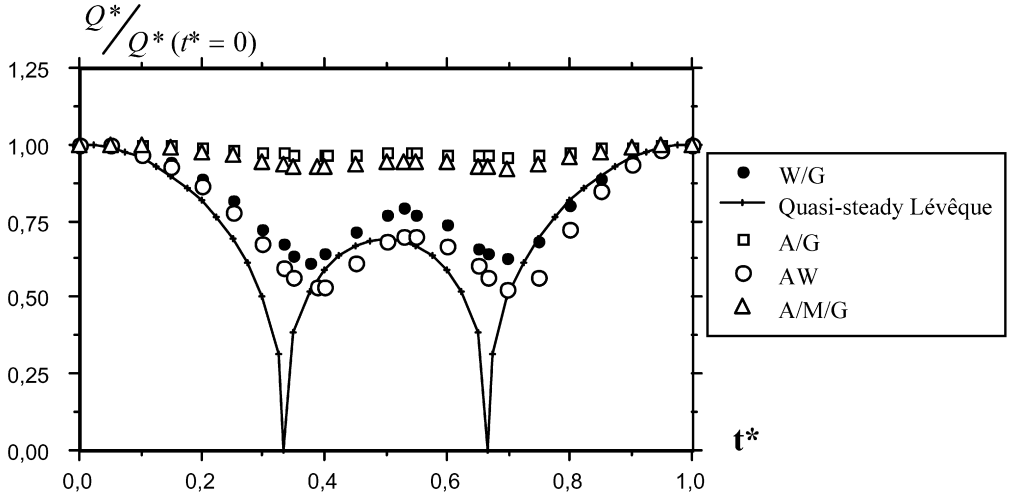

Fig. 8. Ratio of the cyclic variation of the global heat transfer to the transfer at the beginning of the cycle with conduction to the substrate for adiabatic wall (AW), Water/Glass (W/G), Air/Glass (A/G), and Air/Mylar/Glass (A/M/G) configurations. $\omega^* = 0.93.\sigma = 10$, $a = 2$.

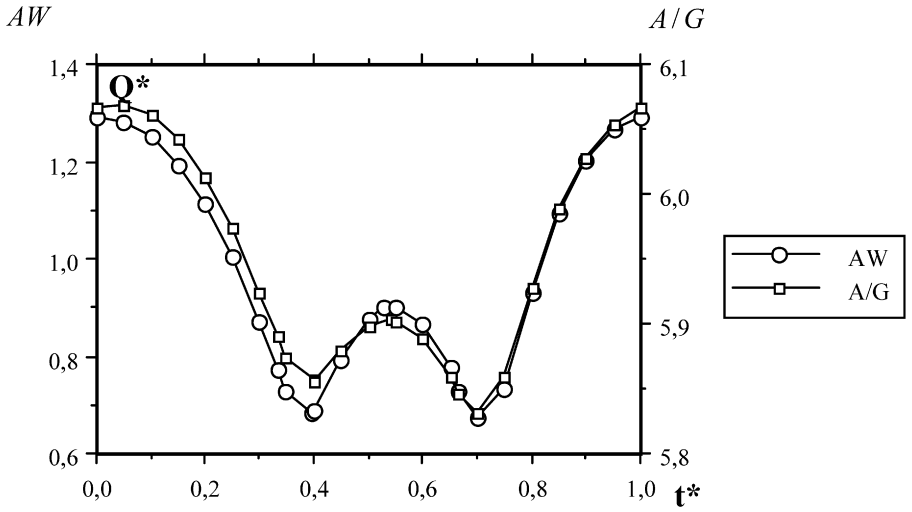

Fig. 9. "Zoom" on the cyclic variation of global transfer for the Air/Glass combination compared with the adiabatic wall (AW). $\omega^* = 0.93$, $\sigma = 10$, $a = 2$.

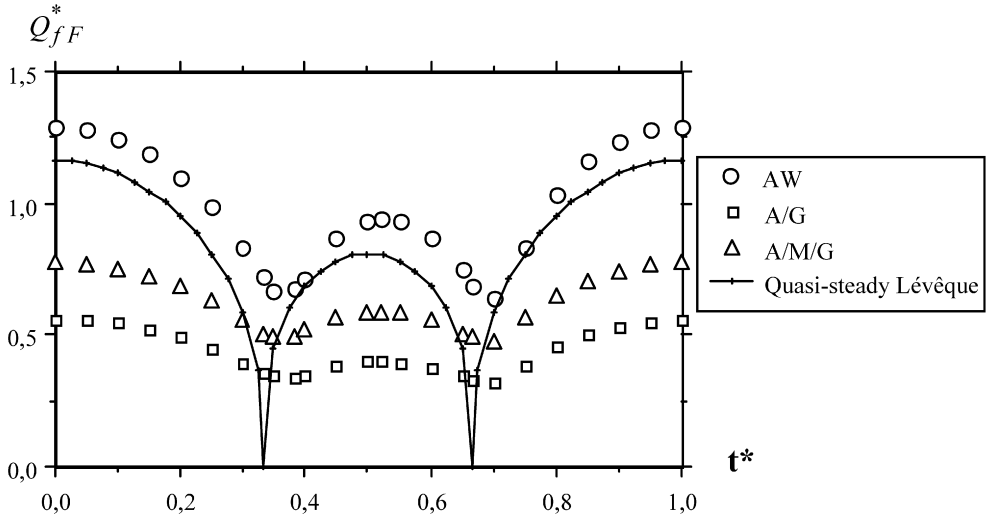

Fig. 10. Modulation of the transfer from the film to the fluid for several substrate configurations. $\omega^* = 0.93$, $\sigma = 10$, $a = 2$.

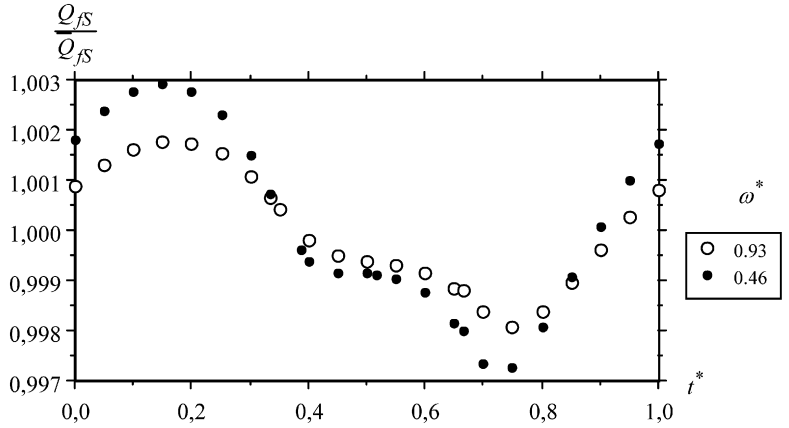

Fig. 11. Modulation of the transfer from the film to the substrate in A/G configuration. $\sigma = 10$, $a = 2$.

according to the classical law $Q_{fF} = A\sigma^{1/3}$, as one would proceed in real experiments. The coefficient A is determined at $\sigma = 30$ from the numerical results and the cyclic modulation of σ is subsequently computed. The resulting σ in the reversal phase is "rectified" by symmetry to the $\sigma = 0$ line. It is seen that the curves collapse reasonably well and that the differences between different configurations are of lesser importance at $\omega^* = 0.93$. A constant temperature anemometer measures

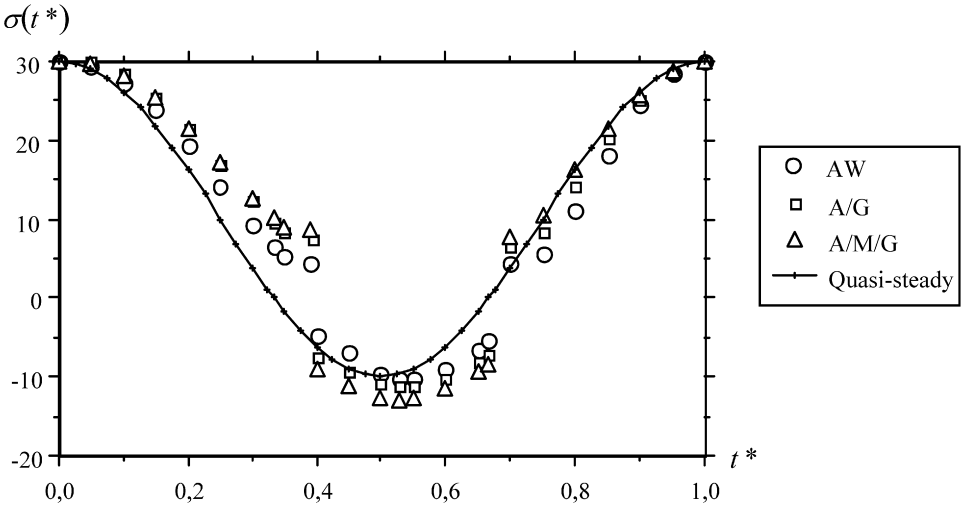

Fig. 12. Shear stress modulations obtained from the direct transfer from the film to the fluid. See the text for the procedure used to convert the direct transfer to the shear. $\omega^* = 0.93$, $\sigma = 10$, $a = 2$.

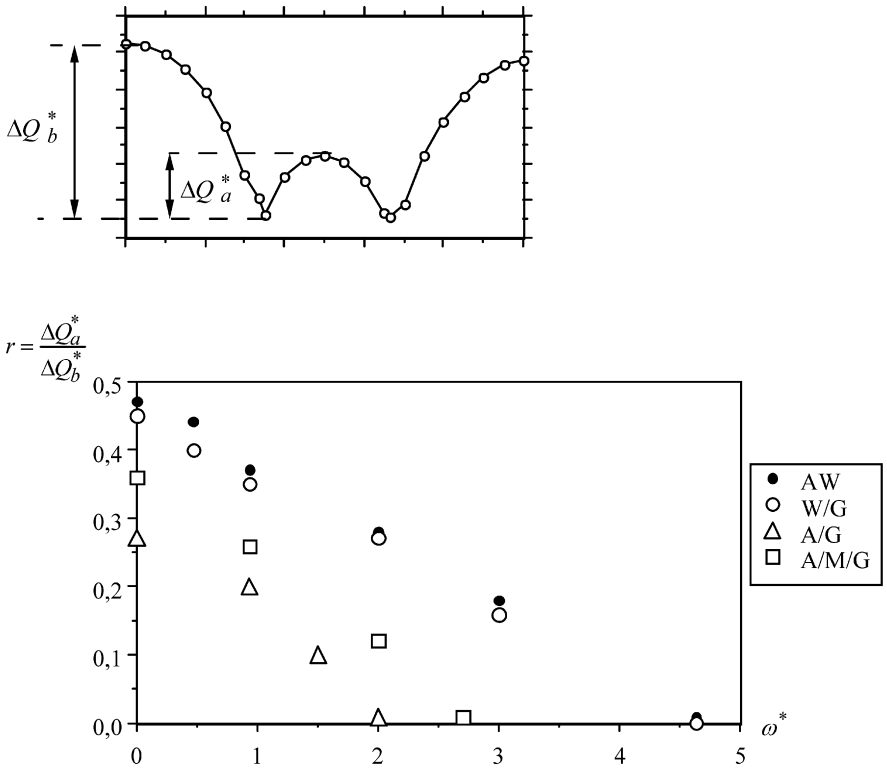

Fig. 13. Variation of the ratio $r = \frac{\Delta Q_a^*}{\Delta Q_b^*}$ versus the imposed frequency defining the cut-off of flow reversal phase determination. $\sigma = 10$, $a = 2$.

unfortunately the total heat flux, and the main difficulty is to extract instantaneously the direct transfer Q_{fF} from Q.

Thus, for small-imposed frequencies $\omega^* < 1$ the flow reversal is detectable from the cyclic variations of from the cyclic variations of $\langle Q^* \rangle$ even at large conductivity ratios $\frac{k_S}{k_F} = 25$. This is no more the case for larger ω^*. More computations have been performed to clearly determine the frequency domain in which the phase of flow reversal can be detected from $\langle Q^* \rangle$. A quantitative criterion has been introduced for this purpose, through the parameter $r = \frac{\Delta Q_a^*}{\Delta Q_b^*}$. Here, ΔQ_a^* and ΔQ_b^* are respectively the raises in amplitude after and before the first flow reversal. This is schematically shown on the top of Fig. 13. The value of r corresponding to the quasi-steady Lévêque solution is $r = 0.66$ in the present conditions with $\sigma = 10$ and $a = 2$. Fig. 13 shows r versus the imposed frequency ω^* for several substrate configurations, including the case for the adiabatic wall (model A) with axial diffusion. It is seen that the "cut-off" frequency corresponding to $k_S = 0$ is roughly $\omega^* = 4.5$. The $\frac{\partial^2 \theta}{\partial x^2}$ term attenuates more rapidly the flow reversal phase than the thermal inertia and wake effects as discussed before.

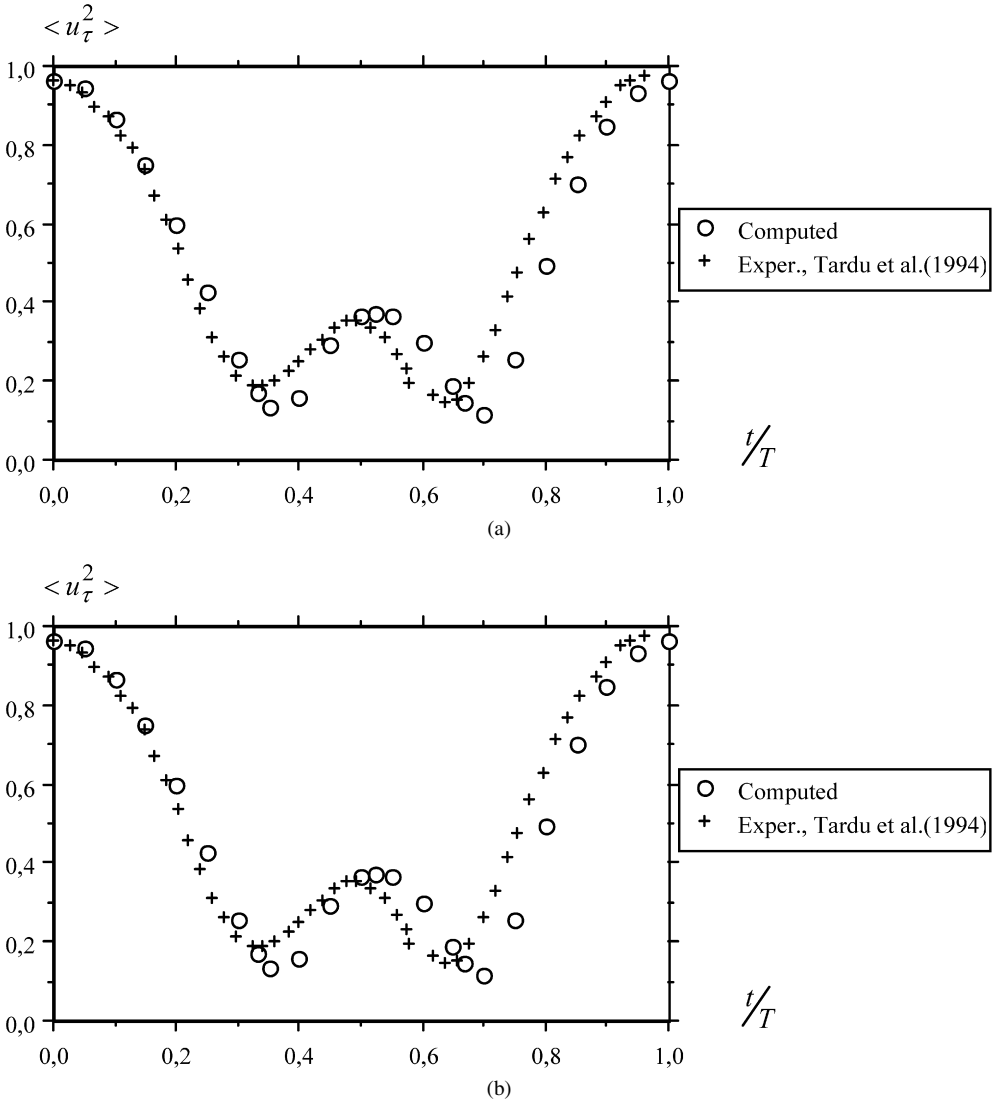

Fig. 14. Comparison with experiments, $\bar{\sigma} = 10$, $a = 2$, $a - \omega^* = 0.46$, $b - \omega^* = 0.93$.

There are only slight differences between $k_S = 0$ and a low conductivity ratio substrate (AW) $\frac{k_S}{k_F} = 1.3$. To give an idea for a real physical situation, note that the Kolmogoroff frequency is $\omega_K^* = 2\pi f_K^* = 60$ in a turbulent fully developed water channel flow with a Reynolds number based on the half channel height of 10^4. Thus, instantaneous turbulent flow reversal can only be detected in the production range in this situation. Indeed successful measurements of phase averaged wall shear stress by flush mounded hot film anemometry have been obtained under flow reversal conditions in a forced wall flow for imposed frequencies up to the mean bursting frequency. That will be discussed in the next session. For a high conductivity ratio (A/G, $k_S/k_F = 25.3$) the cut-off frequency decreases by a factor 2 up to $\omega^* \approx 2$. The detection of flow reversal phase is now more seriously limited. Consider for example a turbulent boundary layer in air with $\hat{u}_\infty = 4$ m/s and a Reynolds number based on the boundary layer thickness of $Re = 10^4$. The Kolmogoroff frequency is roughly 2 kHz in this case. The dimensionless frequency $\omega^* = 2$ at which it is no more possible to depict the flow reversal from $\langle Q^* \rangle$ is only 60 Hz. The isolating thin mylar film improves only slightly the response. The parameter r is suitable because it translates what an experimentalist would see in the measured phase average of the wall shear stress. It has to be noted that, the amplitudes ΔQ_a^* and ΔQ_b^* decrease significantly under the conduction to the substrate but their ratio is relatively less sensitive. For A/G for example ΔQ_a^* and ΔQ_b^* are respectively 5 and 3 times smaller than AW at $\omega^* = 0.93$, but the relative value r differs only by a factor 1.7.

5. Comparison with experiments

The numerical results of the Water/Glass case are compared with the experiments conducted in the unsteady water channel presented before. The procedure of comparison is similar to the determination of the shear from the computations, as we just have discussed. The global heat flux is considered since that is the quantity, which is really measured. The calibration law is $Q = Au_\tau^{2/3} + B$, where it is recalled that u_τ is the shear velocity.

The coefficients A and B are determined at two points far away from reversal points where Q behaves quasi-steadily. Then, the numerical Q is converted to u_τ^2 by using the couple (A, B).

Figs. 14(a) and (b) show the phase average of measured and computed $\langle u_\tau^2 \rangle$ for respectively $\omega^* = 0.46$ and $\omega^* = 0.93$. It is seen that there is an excellent agreement with the measurements especially for the $\omega^* = 0.93$ case. The minimums of the measured shear at the reversal points coincide well with the predictions: that shows the importance of both the axial diffusion and the conduction to the substrate as we discussed in detail in the preceding sessions. The computed shear collapse also well with the measured one before, during and after the flow reversal.

6. Conclusion

Full 2D heat transfer equations concerning the response of a hot film with axial diffusion and conduction to the substrate are numerically resolved in the presence of reversing flow. It is shown that the longitudinal diffusion important during the phase of flow reversal, particularly when the mean Péclet number is small or moderate (30–10), and its contribution to the instantaneous Nusselt number may amount to 40% for moderate frequency. The inertia causes time lags of the thermal boundary layer with respect to the shear. Due to the contribution of longitudinal diffusion, and thermal inertia, as well as the wake swept back over the film during reversal the instantaneous heat transfer curve, is completely different from the simply rectified Lévêque solution curve, at high frequency. It seems difficult, if not impossible, to deduce the instantaneous wall shear stress from the heat transfer from the hot film, with sufficient accuracy under these circumstances.

The conduction to the substrate attenuates considerably the wall film response. For an imposed frequency of about $\omega^* = 1$ and imposed amplitude of $a = 2$ the cyclic variations are reduced by respectively 20 and 7 in the cases Air/Glass and Air/Mylar/Glass. The rectified signal has important second harmonics and the modulation of the measured shear looses his sinusoidal character even at small frequencies such as $\omega^* > 10^{-3}$. The direct transfer from the film to the fluid is also attenuated respectively by 50% and 70% for the cases quoted to before. There is however an acceptably good response when the conductivity ratios of the substrate to the fluid is about one. Thus, in the case Water/Glass, the flow reversal is perfectly detectable from the hot film measurements and there is a good agreement between the measurements and the numerical results for moderate frequencies $\omega^* < 1$. These effects have to be taken into account in the design of micro-sensors with MEMS technology.

References

[1] S. Tardu, G. Binder, R.F. Blackwelder, Turbulent channel flow with large-amplitude velocity oscillations, J. Fluid Mech. 267 (1994) 109–151.

[2] T.J. Pedley, On the forced heat transfer from a hot film embedded in the wall in two-dimensional unsteady flow, J. Fluid Mech. 55 (2) (1972) 329–357.

[3] T.J. Pedley, A thermal boundary layer in a reversing flow, J. Fluid Mech. 67 (1975) 209.

[4] T.J. Pedley, Heat transfer from a hot film in reversing shear flow, J. Fluid Mech. 78 (1976) 513–534.

[5] W.A. Seed, N.B. Wood, Use of a hot film velocity probe for cardiovascular studies, J. Phys. E, Sci. Instrum. 3 (1970) 377–384.

[6] P. Kaiping, Unsteady forced convective heat transfer from a hot film in non reversing and reversing shear flow, Int. J. Heat Mass Transfer 26 (4) (1983) 545.

[7] G.D. Raithby, K.E. Torrance, Upstream-weighted differencing schemes and their application to elliptic problems involving fluid flow, Comput. Fluids 2 (1974) 191–206.

[8] E. Kalnay de Rivas, On the use of nonuniform grids in finite difference equations, J. Comput. Phys. 10 (1972) 202–210.

[9] S. Tardu, P. Pham, Response of wall hot-film gages with longitudinal diffusion and conduction to the substrate, J. Heat Transfer 127 (2005) 812–819.

[10] S.G. Springer, T.J. Pedley, The solution of heat transfer problems by the Wiener–Hopf technique. Leading edge of a hot-film, Proc. Roy. Soc. Lond. A 333 (1973) 347–362.

[11] S.C. Ling, Heat transfer from a small isothermal spanwise strip on an insulated boundary, ASME J. Heat Transfer C 85 (1963) 203–235.

[12] S.G. Springer, The solution of heat transfer problems by the Wiener–Hopf technique. Trailing edge of a hot-film, Proc. Roy. Soc. Lond. A 337 (1974) 395–412.

[13] B.J. Bellhouse, D.L. Schultz, The measurement of fluctuating skin friction in air with heated thin-film gauges, J. Fluid Mech. 32 (1968) 675–680.

[14] P. Freymuth, Sine wave testing of non-cylindrical hot-film anemometers according to Bellhouse–Shoultz model, J. Phys. E: Sci. Instrum. 10 (1980) 705–710.

[15] C.J. Teo, B.C. Khoo, Y.T. Chew, The dynamic response of hot-wire anemometer: IV. Sine wave voltage perturbation testing for near-wall hot-wire/film probes and the presence of low-high frequency characteristics, Meas. Sci. Technol. 12 (2001) 37–51.

[16] D. Meunier, S. Tardu, D. Tsamados, J. Boussey, Realization and simulation of wall shear stress integrated sensors, Microelectron. J. 34 (2003) 1129–1136.

[17] J. Kim, P. Moin, R. Moser, Turbulence statistics in fully developed channel flow at low Reynolds numbers, J. Fluid Mech. 177 (1987) 133–166.

[18] S. Tardu, G. Binder, Response of turbulence to imposed oscillations of high frequencies, Phys. Fluids 5 (1993) 2028–2037.

[19] S. Tardu, G. Binder, R.-F. Blackwelder, Wall shear stress measurements in reversing oscillatory turbulent boundary layers, in: Euromech 202 Conference on Measurement Technique in Low-Speed Flows, 7–10 October, N.L.R., Netherlands, 1985.

[20] R.C. Ackerberg, R.D. Patel, S.K. Gupta, The heat/mass transfer to a finite strip at small Péclet numbers, J. Fluid Mech. 86 (1978) 49–65.